Journal of Asian Earth Sciences 218 (2021) 104847

Contents lists available at ScienceDirect

Journal of Asian Earth Sciences

journal homepage: www.elsevier.com/locate/jseaes

Coulomb stress changes triggering surface pop-up during the 2016 Mw 6.4 Meinong earthquake with implications for earthquake-induced mud diapiring in SW Taiwan

Hue Anh Mai [a,b], Jian-Cheng Lee [b,*], Kate Huihsuan Chen [c], Kuo-Liang Wen [d]

[a] Taiwan International Graduate Program (TIGP) — Earth System Science Program, Academia Sinica and National Central University, Taiwan
[b] Institute of Earth Sciences, Academia Sinica, Taipei, Taiwan
[c] Department of Earth Sciences, National Taiwan Normal University, Taipei, Taiwan
[d] Department of Earth Sciences, National Central University, Chungli, Taiwan

ARTICLE INFO

Keywords:
Mud diapir
2016 Meinong earthquake
Coulomb stress changes
Earthquake triggering
Seismic hazard
Taiwan

ABSTRACT

We investigated the 2016 Meinong earthquake (Mw 6.4) in southwestern Taiwan, which caused surface pop-up in an area of 10x15 km^2 with maximum uplift of 12 cm, where lies an array of mud volcanoes and possible underlying mud diapir. We calculated 3D strain tensor in a 3D mesh with 5x5x2 km grids in the epicentral area induced by the Coulomb stress change due to coseismic fault slip. We obtained substantial contraction strain (10^{-5}–10^{-6}) that occurred in a lobe showing "squeezing" at the depth of 5–14 km below the surface pop-up area. Dilatation strain (10^{-5}–10^{-6}) occurred at shallow level (0–3 km) with a radial pattern around the surface pop-up area. Combining with local geology, which is composed of Mio-Pliocene ~5-km-thick mudstone in a fold-thrust belt, we interpret that the 2016 Meinong coseismic surface pop-up was closely related to mud diapirs/volcanoes, which were likely reactivated by sudden increase of fluid pore-pressure in the basal reservoir (at 5–6 km depth) and dilatation in the shallow level. We also explored the potential effects of the Coulomb stress transfer on nearby receiver faults – including three arrays of mud diapir, the regional decollement, a suspected backthrust and one thrust close to the pop-up area. Our results show that the Coulomb stress transfer a) favors NNE-trending mud diapirs in the coseismic pop-up area, with a combination of clamping stress changes at 5–6 km depth and unclamping stress changes at 0–4 km depth, and b) it does not favor triggered thrust slip on the regional thrusts.

1. Introduction

Mud diapirs/mud volcanoes (MDs/MVs) are commonly found in the areas where rapid sedimentation and tectonic deformation both dominantly prevailed (Westbrook and Smith, 1983; Barber et al., 1986; Yassir, 1989). They have been observed worldwide especially in accretionary wedges such as the Nankai trough, the eastern Mediterranean Sea, south of Timor, southwestern Taiwan, etc. Many argued that abnormally high pore fluid pressures coupled with thick poorly consolidated deposits can facilitate the occurrence of MDs/MVs in accretionary wedge (Kopf, 2002; Deville et al., 2003). Plumbing system of MDs/MVs leads to vertical advection and upward flow of fluid, gas and mud (Brown, 1990). In the tectonically active areas, the interplay between MDs/MVs activity and earthquake faulting has been often anticipated or suspected. Following large earthquakes, suddenly vigorous activities of MVs were observed in many places in the world (Manga et al., 2009; Bonini et al., 2016). On the other hand, MD/MV also manifests its activities during inter-seismic period. The role of MDs/MVs in the sediment deformation becomes a hidden but important issue for regional seismic hazard assessment.

Earthquake-induced mud volcano eruptions have been successfully explained by static stress triggering (Manga and Bonini, 2012; Babayev et al., 2014; Bonini, 2019). Due to stress changes or transfers, the hydraulic properties surrounding the mud source could be altered. The mud/fluid/gas intrusive processes (i.e., MD or MV), therefore, can be affected by the sudden stress change from nearby earthquakes. Bonini et al. (2016) calculated the statistic stress changes on mud dyke feeder systems of MVs in four different tectonic environments around the world, including Azerbaijan, Romania, Italy, and Taiwan. They established a critical role of the stress triggering on the mud eruptions,

* Corresponding author.
E-mail address: jclee@earth.sinica.edu.tw (J.-C. Lee).

https://doi.org/10.1016/j.jseaes.2021.104847
Received 22 September 2020; Received in revised form 10 May 2021; Accepted 27 May 2021
Available online 31 May 2021

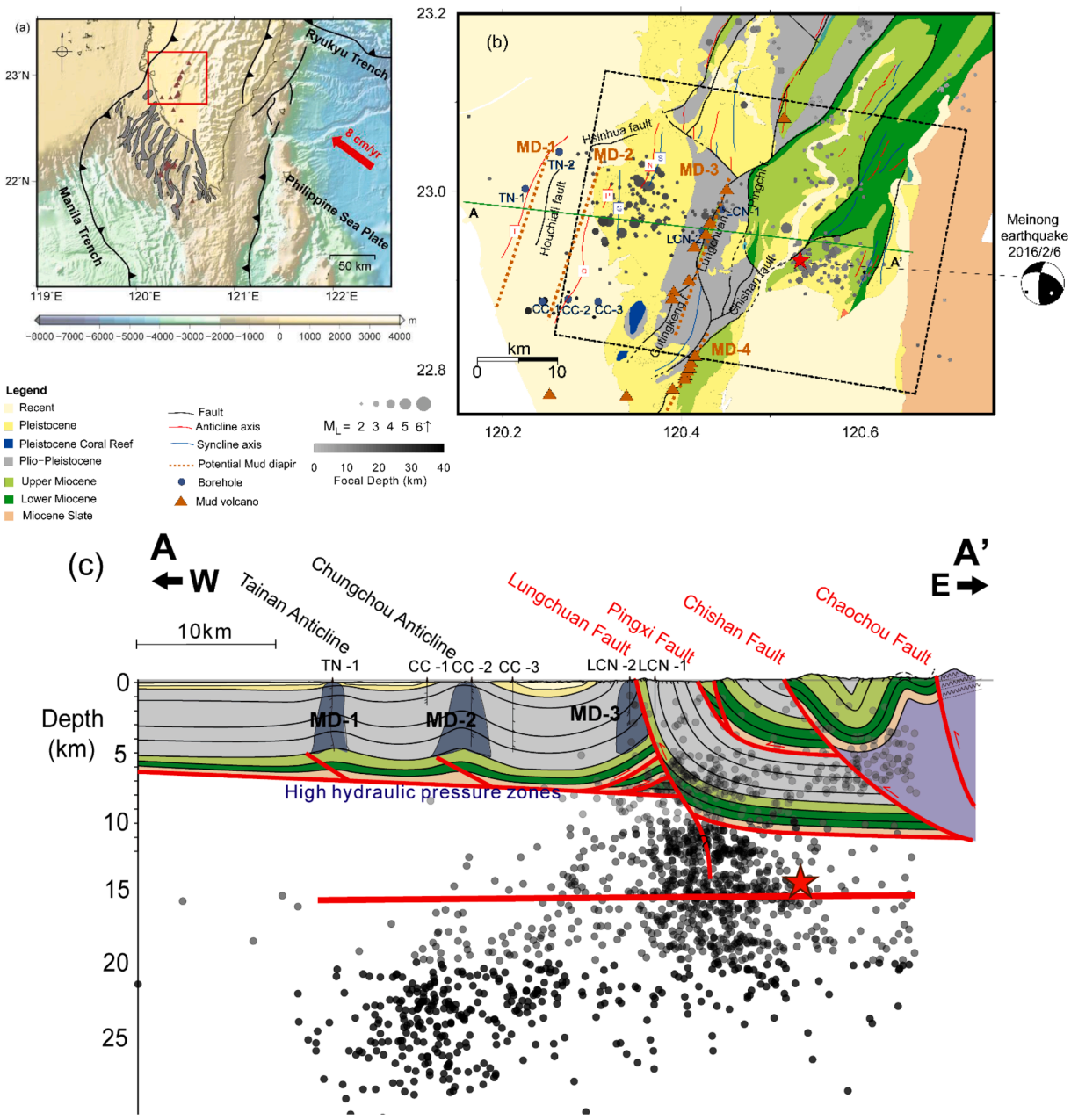

Fig. 1. a) Geodynamic setting of southwestern Taiwan. The southwestern Taiwan is located in the transition between the collision of Philippine Sea plate against Eurasia and the subduction of South China Sea along the Manila trench. Several arrays of mud diapirs (gray areas) /mud volcanoes (brown triangles) have been identified in the accretionary wedge in the offshore of SW Taiwan, which appear to extend into inland fold-thrust belt; b) Geological map of southwestern Taiwan (modified from Chinese Petroleum Corporation CPC, 1989). The mainshock (red star) and the aftershocks (gray dots) (within 1 month) of the 2016 Mw 6.4 Meinong earthquake are shown on the map. The focal mechanism was determined by centroid moment tensor (CMT) from BATS network. The dash black rectangle indicates the surface projection of the source fault model of the main shock from Lee et al., 2016. MD-1, MD-2, and MD-3 represent three potential mud diapirs arrays in the area. c) General geological cross-section across the epicentral area (after Peng et al. (2020)). The deformation structure is characterized by a fold-thrust belt with a decollement estimated at the depth of 6–8 km. However, the development of several regional anticlinal folds might be closely related to the vigorous mud diapiring. (For interpretation of the references to color in this figure legend, the reader is referred to the web version of this article.)

emphasizing compression of the mud source in the deeper part and stress unclamping on shallower conduit of mud volcanos.

Following the co-seismic displacements on ruptured faults comprehensively evaluated by the half-space dislocation model Savage and Prescott (1978), Okada (1985) and Okada (1992) generated a compact, state-of-the art analytical expression for calculating surface deformation due to shear and tensile stresses in a half-space fault. The co-seismic slip distribution on ruptured fault(s) can thus be calculated via Okada's formula, usually inverted from surface geodetic data or seismological information, based on the Coulomb stress change (Reilinger et al., 2000; Jónsson et al., 2002; Ching et al., 2011; Hsu et al., 2011; Serpelloni et al., 2012; Huang et al., 2016). Following Okada's formula earthquake-induced volumetric strain has been also calculated during large earthquakes (Quilty and Roeloffs, 1997; Johnston et al., 2006; Shi et al., 2013). Such co-seismic volumetric strain leads to a perturbation in pore pressure in the rocks and therefore alters the state of stress in the Earth's crust. The predicted volumetric strain and the observed change of water table at wells in the epicentral area of earthquakes were found to be consistent, to some extent, with each other in several previous studies (Albano et al., 2017; Kroll et al., 2017). However, mismatches

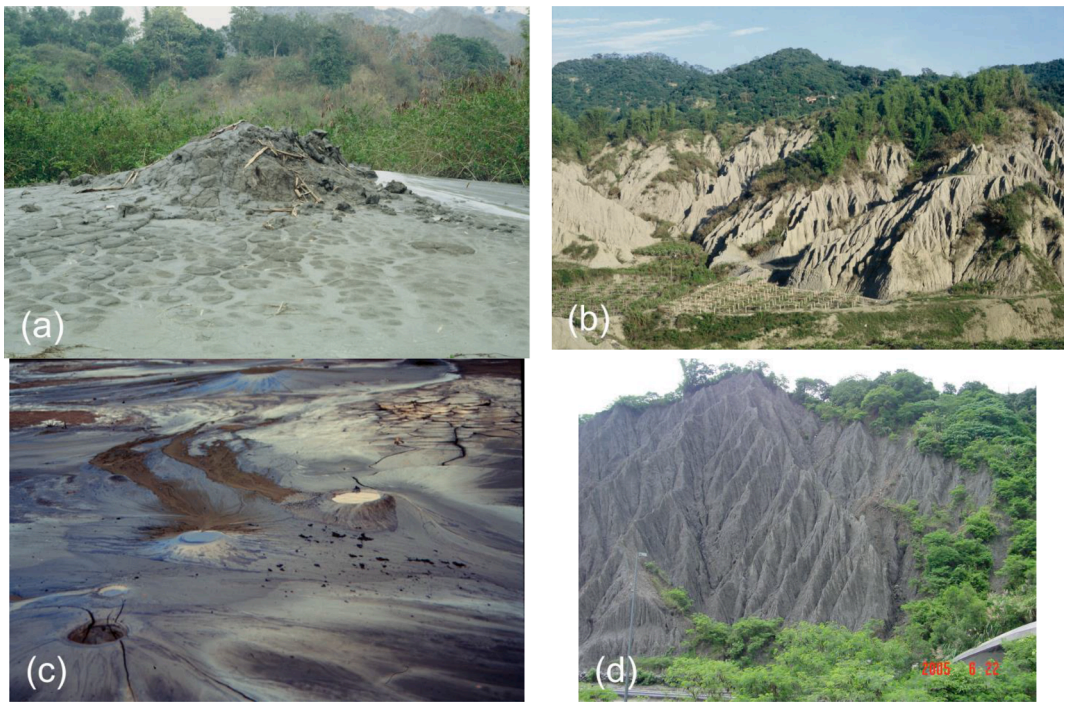

Fig. 2. Photographs of mud volcanoes and badlands in the mudstone area of the southwestern Taiwan. a) Wushanding mud volcano (22.7960° N, 120.4060° E) with cone-shape in the Tianliao area; b) Panorama view of landscape in the mudstone area; c) Field photograph of small mud volcanoes (22.87826° N, 120.38998° E) with craters on the top in the Tianliao area; d) Badland of mudstone, showing poorly consolidated rocks with strong surface erosion features in the Lungchi area.

sometimes existed. They are likely due to uncertainties in the parameters of the source fault model (Qiu and Shi, 2003) or the complexity and heterogeneity of the rocks and hydraulic systems in the shallow crust (Grecksch et al., 1999; Weaver et al., 2019).

An accretionary system in the southwestern Taiwan is located in a transition zone from the subduction of the South China Sea to the collision between the Eurasian continent and the Philippine Sea to the north (Teng, 1990; Liu et al., 1997; McIntosh et al., 2005; Ku and Hsu, 2009; Kuo-Chen et al., 2012). Due to enormous erosion from rapid mountain building in the past 2–3 million years, more than 5 km thick mudstone rock units were distributed from the onshore area to the offshore area in southwestern Taiwan (Li, 1976; Suppe, 1981; Chang and Chi, 1983; Liu and Yu, 1990; Teng, 1990; Dadson et al., 2003). In this mudstone dominated area, the geological structures are mainly characterized by a series of NNE-trending thrust faults and folds (Fig. 1), as a result of northwestward collision of the Luzon arc and the Philippine Sea plate. The tectonic compression of the over-pressured sediment and fluid leads to a series of inland and offshore active MDs/MVs (You et al., 2004; Chao et al., 2011; Doo et al., 2015; Ching et al., 2016). Several arrays of MDs/MVs were documented in the offshore region of southwestern Taiwan based on a rich volume of seismic-reflection data (Liu et al., 2006; Chen et al., 2014; Doo et al., 2015). In addition, the offshore MDs/MVs are found to align with the inland ones (Chiu et al., 2006; Hui et al., 2018). It is crucial to understand whether the presence of MDs in the inland fold-thrust belt plays some roles during earthquakes and how MDs and folds and thrusts interplay with each other.

On 6 February 2016, the Mw 6.4 Meinong earthquake occurred in southwest Taiwan, at a depth of about 15 km (mainshock and aftershocks are shown in Fig. 1). The most obvious coseismic surface deformation observed from GPS and Interferometric Synthetic Aperture Radar (InSAR) was characterized by a pop-up area of about 10 x15 km with a peak uplift of 12 cm, although without a clear responsible surface geological fault. This co-seismic uplift area coincides with the mudstone area where a series of mud volcanoes (with possible underneath mud diapir) that are aligned along with the regional NNE-trending fold-thrust structures. There were mud eruptions being observed during the Meinong earthquake: the Wushanting mud volcano (22.7960° N, 120.4060° E), which is located on the southern edge of the surface pop-up area, and the Nanhua mud volcano (23.0816° N, 120.5170° E), which is located at 10–15 km north of the epicentral and pop-up area. Does the MD/MV activity contribute to the co-seismic surface pop-up deformation? In this study, we intend to quantitatively characterize the volumetric strain change due to the co-seismic rupture of the 2016 Mw 6.4 Meinong earthquake fault in southwestern Taiwan. Precisely, we aim at studying the possible cascade effects from co-seismic fault slip induced stress change, volumetric strain change, pore-pressure increase and mud diapiring, to surface pop up. By comparing the volumetric strain change with the architecture of (1) the local fold-thrust system (including the decollement) and (2) the network of fluid/gas conduits of the mud volcanoes at the depth, we propose some plausible explanations for the co-seismic uplift in this area, which is potentially helpful for seismic hazard mitigation.

2. Tectonic and geological setting

The Taiwan orogenic belt is an ongoing arc-continent collision where the oblique convergence has been occurring between the Luzon volcanic arc of the Philippine Sea plate and the passive continental margin of the Eurasian plate since 5–6 Ma (Suppe, 1981; Teng, 1990; Ho, 1982). On the other hand, the southwestern Taiwan is situated in the transition zone from the aforementioned collision in the north, to the subduction of South China Sea under Luzon (remnant of pull-apart Eurasian margin) in the south. To a lesser degree, SW Taiwan is also affecting by the southwestward lateral extrusion (Lu and Malavieille, 1994; Angelier et al., 2009). Our study area is located in the southern end of the Western Foothills of the Taiwan mountain belt (Fig. 1a). The surface geological rock units are composed of shallow marine deposits (Miocene) and transition sequences from shallow marine to terrestrial deposits (Plio-Pleistocene) (Fig. 1b). One striking feature in this region is the widespread poorly consolidated mudstone, exhibiting badland landscape (Fig. 2). These ~5 km thick mudstone units resulted from the rapid accumulation in foreland basin in response to the mountain building of

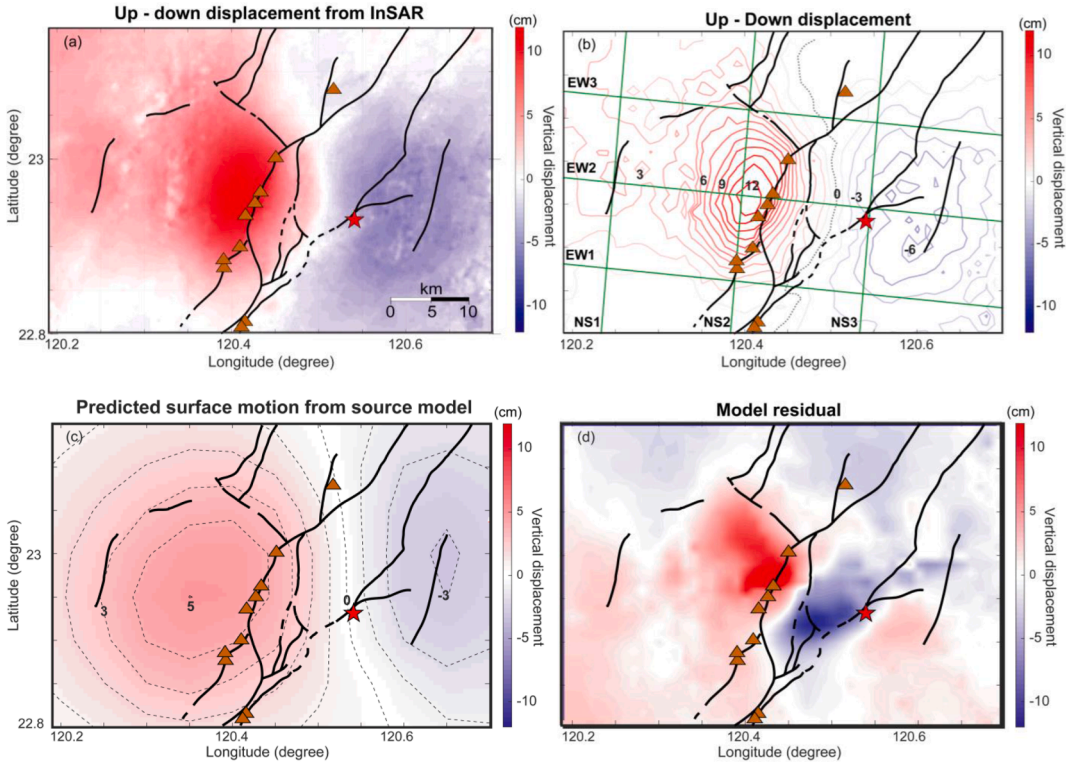

Fig. 3. Coseismic vertical deformation of the 2016 Mw6.4 Meinong earthquake (a) color coded and (b) contour lines (number in cm), derived from InSAR analyses (after Huang et al., 2016). The coseismic vertical deformation is characterized by a pop-up area of 15x10 km (red area) with the maximum uplift of 12 cm and a subsidence area with the maximum of −6 cm (blue area). Green lines indicate the vertical profiles for illustrating the coseismic strain change. c) Vertical displacement at surface (0 km) obtained from forward calculation by the fault slip model proposed by Lee et al. (2016); d) Model residual between the observed InSAR data (Fig. 3a) and the inverted data from the model (Fig. 3c). (For interpretation of the references to color in this figure legend, the reader is referred to the web version of this article.)

the Central Range during Plio-Pleistocene (Chang and Chi, 1983; Liu and Yu, 1990; Teng, 1990; Dadson et al., 2003).

The regional geological structures of the southwestern Taiwan are characterized by a series of NNE-trending folds and thrusts, generally syncline in the footwall and anticline in the hanging wall of thrust. As shown in Fig. 1c, there are 5–6 pairs of thrust and anticlines, from west to east, including 1) the Tainan tableland (anticline) and the Houchiali fault (a backthrust), 2) the Chungchou anticline and the Chungchou fault, 3) the Takangshan anticline and a possible buried thrust fault, 4) the Lungchuan anticline and the Lungchuan fault, 5) the Pingxi fault, which breaks through an anticline in the hanging wall, and 6) the Chishan fault, which also breaks through the hanging-wall anticline. A decollement of this fold-thrust belt has likely been developing at the depth of around 6 to 8 km (Mouthereau et al., 2001; Ching et al., 2016; Le Béon et al., 2017).

Four major groups of mud diapirs, which is a sort of network of sub-vertical fractures and pipes stemming from the cores of regional major anticlines and forming the plumbing of mud volcanoes, have been proposed in Southwest Taiwan (Fig. 1b and 1c), from west to east: 1) MD-1 at the Tainan tableland, 2) MD-2 at the Chungchou anticline, 3) MD-3 close to the Lungchuan fault, and 4) MD-4 at the southern part of the Chishan anticline. The MDs/MVs appear to play a significant role on contribution to the active surface deformation in SW Taiwan during the interseismic periods, according to geodetic measurements and field observations (Hsieh, 1972; Ching et al., 2016). Offshore geophysical surveys of seismic reflection also reveal that several arrays of aligned mud diapirs dominate the long-term deformation structure/mechanism of the major anticlines in the offshore area of SW Taiwan (Chiu et al., 2006; Chen et al., 2014). A close structural connection and continuation of anticline/mud diapir between inland fold-thrust belt and offshore accretionary wedge has thus been proposed. How much MDs/MVs activity contribute to the surface deformation (pop-up mud diapiring or fault-related folding)? Can we discriminate the effect of MDs/MVs from that of fold-thrust systems? And what is the role of MDs/MVs on the development of the anticlines associated with the major thrusts? These questions also evoked our motivation to study the possible influence of MDs/MVs on surface deformation during large earthquakes.

3. The 2016 Meinong earthquake

The Meinong earthquake occurred in southwestern Taiwan on 6 February 2016 (03:57 local time, UTC + 8:00) with a moderate/large magnitude, Mw 6.4, that caused severe damages to human construction and life in the region. The epicenter of the main shock, 120.544° E and 22.922° N, was located in the southernmost fold-thrust belt of the Taiwan mountain range (Fig. 1). During the first month following the main shock, the aftershocks were mainly grouped in three sub-areas (Wen et al., 2017). Group A was located surrounding the main shock and at depths ranging from 10 to 20 km (grey circles near the red star in Fig. 1b and 1c). Group B was situated about 20 km west of the main shock at depths of 20–30 km. Group C was less concentrated to the north of the mainshock at depths of 5–15 km. Focal mechanisms for the mainshock calculated from various methods consistently showed shallow thrust-faulting with a substantial strike-slip component. The inferred causative fault is a WNW-trending fault plane dipping 25–30° to the NNE, in a dimension of 45 × 40 km^2 (rectangular in Fig. 1b) from depths of about 8 to 24 km (CWB, 2016; Huang et al., 2016; Lee et al., 2016).

It appears that the focal depth of 14.6 km as well as the associated coseismic fault patch (8–24 km) are all below the decollement of the fold-thrust belt (6–8 km at depth). In the epicentral area, no mapped geological fault on the surface level was identified as the responsible co-

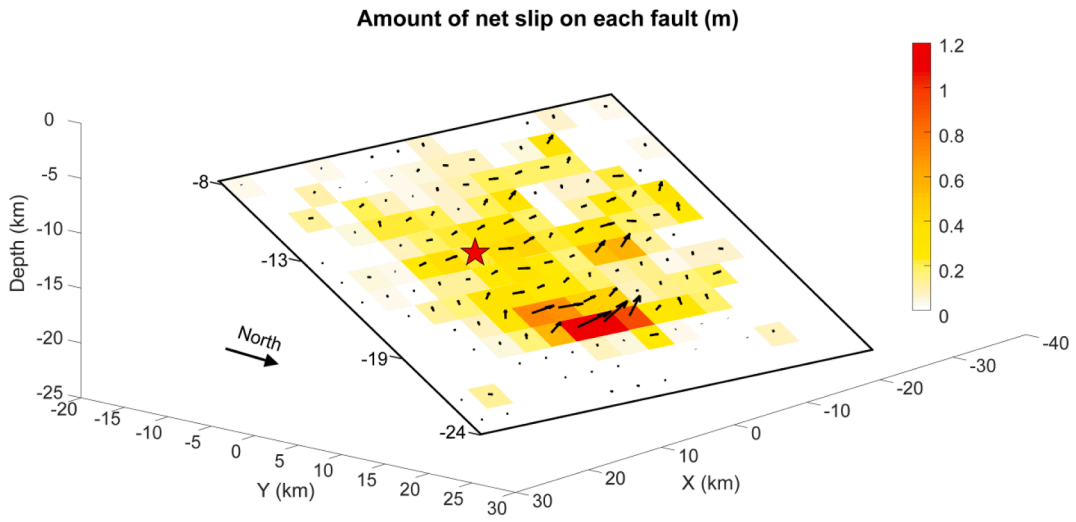

Fig. 4. The model of coseismic slip distribution on the fault of the Meinong earthquake adopted in this study for calculation of Coulomb stress change (after Lee et al., 2016). The fault geometry: strike of N281°E, dip of 24°N and depth of 8–24 km. Red star: main shock. (For interpretation of the references to color in this figure legend, the reader is referred to the web version of this article.)

seismic fault, although surface fissures or ruptures on man-made structures were found in several places, particularly at Kuanmiao town (Le Béon et al., 2017). The InSAR results indicate an uplift up to 12 cm distributed over a 15 km × 10 km area (Fig. 3a) (Huang et al., 2016; Le Béon et al., 2017), which represents the largest co-seismic surface deformation that took place about 10–15 km west of the epicenter (Fig. 3b). To east of the epicenter, the InSAR analysis reveals subsidence down to −6 cm in a 10 km × 10 km area. At first glance, the location of the major coseismic uplift area coincides with the mudstone-dominated Gutingkeng formation, where an array of mud volcanoes have been developed (i.e., MD-3). Whether the surface pop-up deformation can be induced by coseismic slip on a deeper causative fault or other possible structures and what is its potential implication on mud diapiring are the issues addressed here.

4. Method: Calculation of coseismic stress and strain changes

We computed the Coulomb stress change (ΔCFS) in order to understand the influence of co-seismic slip on surrounding structures. The ΔCFS induced by fault rupturing of an earthquake (positive means failure being promoted) can be written as (Stein and Lisowski, 1983; Stein et al., 1992; King et al., 1994):

$$\Delta CFS = \Delta\tau + \mu' \Delta\sigma_n, \quad (1)$$

where Δτ is the change in shear stress (positive when sheared in the direction of fault slip); $\Delta\sigma_n$ is change in effective normal stress on fault plane (positive or increase means the fault became unclamped); μ' is the effective friction coefficient on the fault plane (we adopted here a value of 0.4 which was commonly used for Earth's crust faulting).

4.1. Calculation of volumetric strain changes

The static Coulomb stress change in the 3-D space induced by the co-seismic slip can be determined on the causative fault with the orientation and geometry of the fault. By applying a fault dislocation model we can calculate the static stress and volumetric strain change generated by an earthquake. We adopted the analytical expressions of Okada (1992) for the internal displacements and strains due to shear and tensile faulting in an elastic half-space for a finite rectangular source.

Based on the previous studies in the literature, we utilized the coseismic slip model of Lee et al. (2016) as the source model (Fig. 4), which was computed from a joint inversion combining teleseismic body waves, GPS coseismic displacements, and local ground-motion waveform records. Lee et al. (2016) claimed that total misfit of this coseismic slip model from the three data sets is 0.34 (varying between 0 and 1), suggesting that the model fit reasonably well with observation data. However, the inverted vertical displacement from the slip model showed residuals occurrence, in particular around the surface pop-up area (Fig. 3c and 3d), compared to the InSAR observation (Huang et al., 2016). We thus suspect that other mechanism(s) involved for the surface pop-up, instead of solely co-seismic fault slip. In this fault model with a strike of 281° and a dip of 24° (Fig. 4), two main asperities are distributed on the fault plane. The largest asperity with the maximum slip amount of 120 cm was located down-dip of the main shock at the depths of 18–20 km. The second largest asperity with slip up to 70 cm was developed at the depth of about 15 km to the west of the main shock.

We calculate the spatial distribution of the co-seismic static volumetric strain using the open-source program Coulomb 3.3 (Lin and Stein, 2004; Toda et al., 2005), which is based on Okada's dislocation theory. With the coseismic slip model in Fig. 4 as the input source, we calculated 3-D tensors of strain change induced by coseismic Coulomb stress change. The mathematical expressions are described as following. The displacement u_i and its space derivative $\partial u_i/\partial x_j$ at an arbitrary point on the Earth surface (or inside of the semi-infinite medium) can be calculated from the coseismic slip model, which is inverted from geodetic measurements and seismic data, allowing us to compute strain tensor (ε_{ij}) and stress field tensor (σ_{ij}) by the following relations:

$$\varepsilon_{ij} = \frac{1}{2}\left(\frac{\partial u_i}{\partial x_j} + \frac{\partial u_j}{\partial x_i}\right) \quad (2)$$

$$\sigma_{ij} = \lambda\, \varepsilon_{kk}\, \delta_{ij} + 2\mu\, \varepsilon_{ij} \quad (3)$$

where λ and μ are elastic constants of the medium; δ_{ij} is Kronecker delta.

By expressing the principal strain axes (ε_{11}, ε_{22}, ε_{33}), we can illustrate the characteristics of the coseismic volumetric strain change in 3-D space. An approximation to the Earth's crust is made by an assumption of an elastic medium, which can be represented by the following elastic moduli: Poisson's ratio $\nu = 0.25$, Young's modulus E = 80 GPa, and coefficient of friction, μ' = 0.4, commonly adopted by geoscientists and modelers (King et al., 1994; Lin and Stein, 2004; Toda et al., 2005; Toda et al., 2011). Nevertheless, we calculated additional tests to investigate the effects of different coefficients of friction, with μ' = 0.3 and μ' = 0.5. The results show no substantial change for vertical surface displacements, strain changes, normal stress changes; but they would

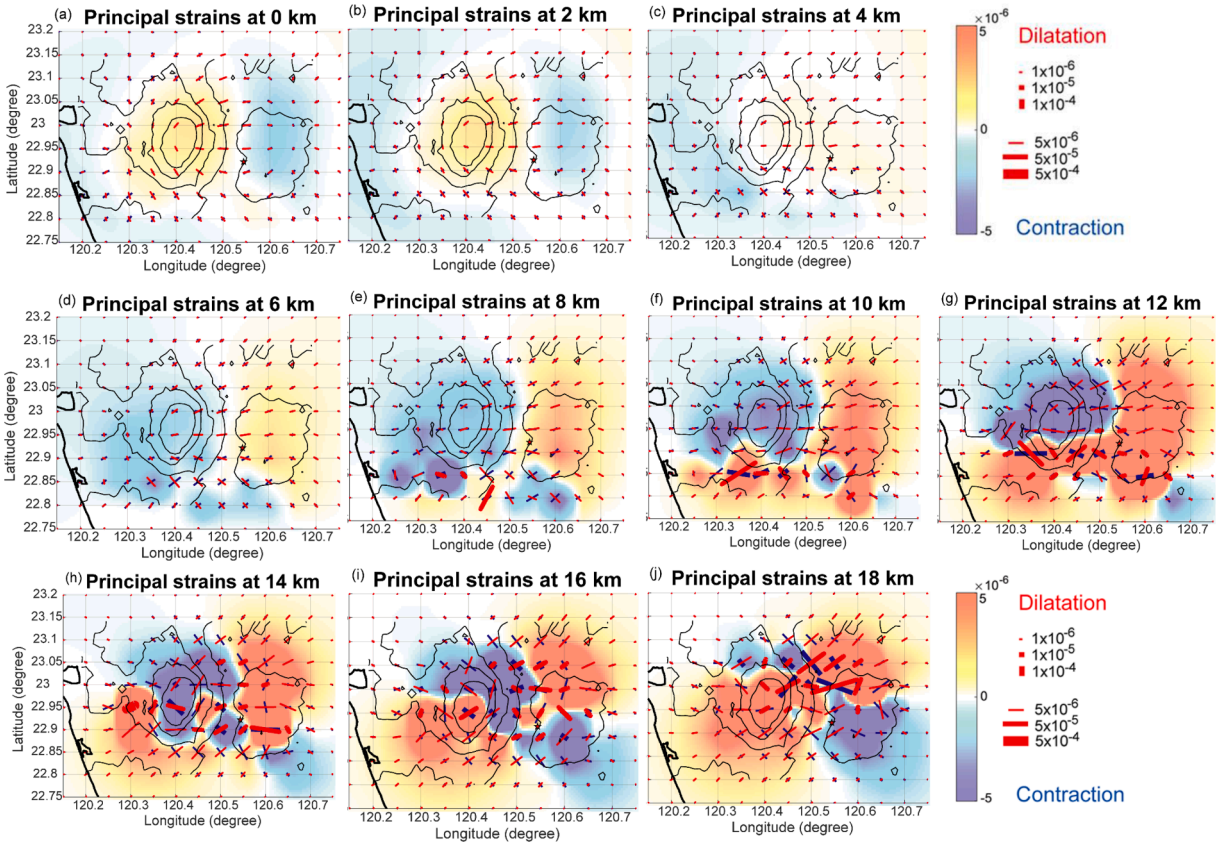

Fig. 5. Results of calculation of volumetric strain changes derived from Coulomb stress change due to coseismic rupturing of Meinong earthquake. Distribution of 3-D principal strain projected on to the horizontal plane with a 5 × 5 km grid. We illustrate the strain at the different depths for each 2 km from 0 to 18 km, (a) to (j), respectively. Red color: dilatation strain. Blue color: contraction strain. The amplitudes and orientations of the principal strain axes are shown in red lines (lengthening) and blue lines (shortening). The contour lines of coseismic pop-up are superimposed in the map for comparison. Black star denotes the epicenter of the 2016 Meinong earthquake. We found a close relation between volumetric strain changes and coseismic surface pop-up: a) substantial dilatation strain with a radial pattern occurred at the shallow 0–2 km in the coseismic pop-up area and b) contraction strain with 'squeeze' character occurred at the depths of 5–14 km beneath the pop-up. We argue that this strain pattern increased the fluid pore-pressure in the root of the mud diapir (5–6 km deep) and promoted the activity. See explanation in detail in main text. (For interpretation of the references to color in this figure legend, the reader is referred to the web version of this article.)

slightly affect the magnitude of Coulomb stress changes on mud diapirs (see details in Fig. A1 in Appendix).

4.2. Calculation of elastic stress transfer

The shear and normal stresses produced by a source earthquake can be resolved on specific 'receiver' faults in terms of Coulomb stress transfer. In order to explore the potential influence or triggered slip on geological structures around the epicentral area, we computed static stress changes induced by the 2016 Meinong earthquake on a few faults/fractures representing potential receiver structures for mud diapirs. For exploring the possibility of triggered mud diapiring, we focused on three major sub-parallel mud diapirs, which were approximated as vertical feeder faults/fractures (MD-1, MD-2, MD-3 in Fig. 1). As mentioned above (Fig. 1c), the MD-1 aligns along with the Tainan tableland; the MD-2 aligns along with the Chungchou anticline; the MD-3 aligns along with the Lungchuan fault. Based on the previous studies on regional geology, alignment of mud volcanoes, the structural relationships between onshore and offshore mud diapirs structures (Liu et al., 1997; Chiu et al., 2006; Hui et al., 2018), the orientation parameters of these mud diapirs are approximated as strike = N10-20°E, dip = 90°, depth = 1–6 km. Note that the three mud diapirs have similar orientations with a width of 1–2 km and extend from near surface to about 4–5 km depth (Chen et al., 2014). In the calculation, an increase of dilatation normal stress would tend to promote unclamping of mud diapir.

In addition to mud diapirs as receiver faults, we also consider other possible triggered structures in the epicentral area, including 1) the regional decollement of fold-thrust belt, 2) a major thrust, the Lungchun fault, close to the surface pop-up area, and 3) a suspected shallow blind back-thrust, proposed in the previous study (Le Béon et al., 2017). The setup parameters will be described in the section of Discussion.

5. Results

5.1. Tensor of strain changes in 3D grids

We determined the tensors of strain change induced by the coseismic Coulomb stress change of the 2016 Meinong earthquake. We divided shallow crust of the study area into a horizontal grid cell of 0.05° × 0.05° (approximate 5 km × 5 km) and in vertical direction each 2 km from depths of 0 to 18 km. The volumetric strain changes induced by coseismic slip are resolved at various depths. Fig. 5 shows the calculated maximum and minimum principle strain axes projected on the horizontal planes at different depths, with background of superimposed InSAR surface vertical displacement (contour lines). In the co-seismic surface uplift area, there exists substantial dilatation strain (yellow/red color, 10^{-5}–10^{-6}) at the shallow depth of 0–2 km, where the shallow contraction strains (blue color, -1 to 3×10^{-6}) coincides with the area of co-seismic subsidence (Fig. 5a and 5b). The strain pattern changes downward to greater depths. Below the co-seismic uplift area, we find significant contraction strain at the depths of 6–14 km (blue color in Fig. 5), which changes again to dilation at 16–18 km (red color).

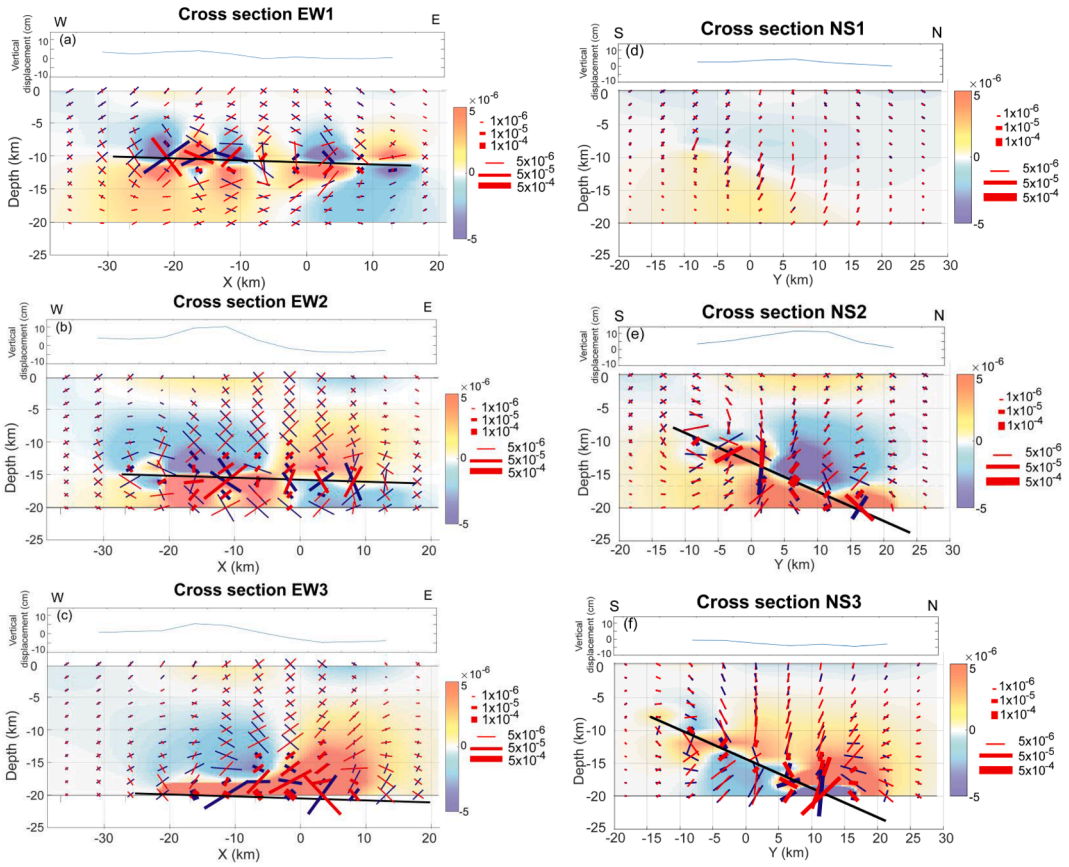

Fig. 6. Results of volumetric strain calculation in the vertical profiles along E-W direction (a), (b), and (c) and along N-S direction (d), (e), and (f). See Fig. 3b for location of the profiles. The coseismic surface vertical displacements derived from InSAR also were plotted in each profile for better comparison. Red color: dilatation strain. Blue color: contraction strain. The amplitudes and orientations of the principal strain axes are shown in red lines (lengthening) and blue lines (shortening). The causative fault of the main shock is indicated as black heavy line. In the surface pop-up area, we can observe dilatation strain occurred at the shallow 0–2 km and contraction strain at the depths of 5–14 km above the coseismic fault (Fig. 6b and 6e). See main text for more detailed descriptions. (For interpretation of the references to color in this figure legend, the reader is referred to the web version of this article.)

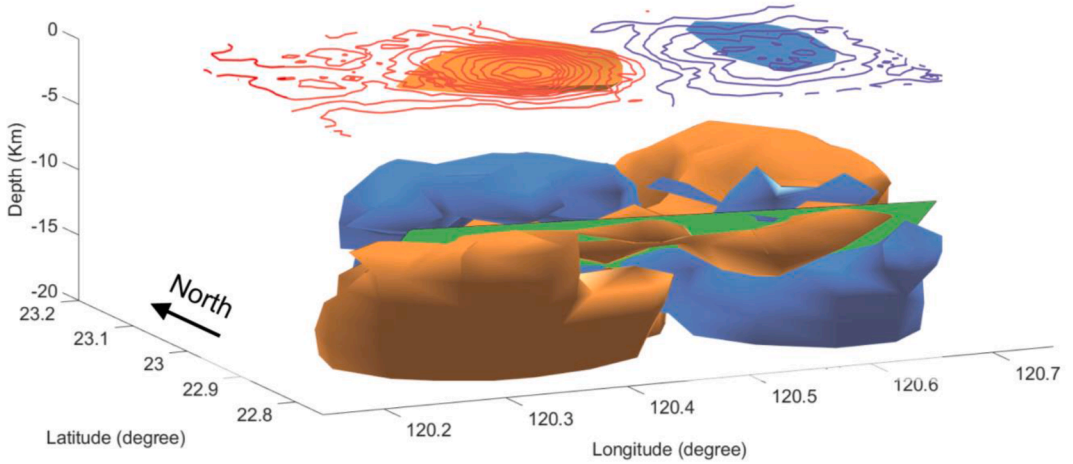

Fig. 7. 3D perspective view of coseismic volumetric strain change induced by the earthquake. Blue color: contraction lobes; orange/red color: dilatation lobes. The causative fault of the mainshock is indicated as green plane. Surface co-seismic vertical deformation (uplift in red and subsidence in blue) are represented in contour form. We can observe that one of the main contraction lobes occurred at the depth of 5–14 km, below the surface pop-up and above the causative fault. (For interpretation of the references to color in this figure legend, the reader is referred to the web version of this article.)

To better view the depth dependency of strain field, we then display the cross-sections along six vertical profiles: EW1-3 and NS1-3 (location indicated in Fig. 3b). As shown in Fig. 6, the two cross-sections of EW2 (perpendicular to regional NNE trend) and NS2 (parallel to regional NNE trend) reveal that the co-seismic fault plane separates the substantial contractional strain (blue color, -1×10^{-5}– to 10^{-6}) to the top from the dilatational strain (red color, 10^{-5}–10^{-6}) to the bottom. Strain pattern changes dramatically from west to east especially from NS2 to NS3,

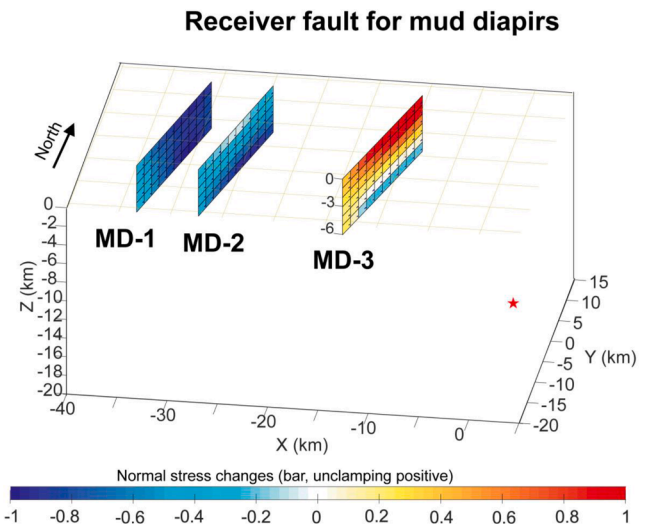

Fig. 8. Results of calculation of Coulomb stress transfer on three arrays of MDs/MVs in the study area (location see Fig. 1b). Note that MD-3 is located in the coseismic pop-up area. These three MDs/MVs are treated as receiver faults for Coulomb stress transfer. Normal stress changes on three mud diapirs are also shown in colors: red color means unclamping for MDs/MVs and blue color indicates clamping. We found that the Coulomb stress transfer might induce clamping in the deeper part (5–6 km) of the MD-3 and unclamping in the shallow 0–3 km. See main text for more explanations. (For interpretation of the references to color in this figure legend, the reader is referred to the web version of this article.)

corresponding to the opposite sign of displacement field across the epicenter (around 120.5°E). The largest strain concentrates near the fault plane.

We also present a 3-D visualization in Fig. 7. The contraction and dilation strain are represented by blue and orange colors, respectively. Below the surface pop-up area, we found a major contraction strain lobe (blue) extending at depth in the range 5–14 km, a few kilometers above the coseismic fault plane (green rectangular). The uppermost part of this depth range is seemingly close to the decollement of fold-thrust belt. We think this is important because it is near the base and reservoir of the regional mud diapir MD-3.

5.2. Characteristics of strain changes vs. coseismic surface uplift area

Our results show co-seismic contraction in the upper crust under the co-seismic pop-up area, as revealed by the principal strain axes projected on to the horizontal plane (Fig. 5) and the vertical profiles (Fig. 6). The lobe of contraction strain (i.e., blue-colored area beneath the surface uplift area at the depth of 5–14 km) exhibits a general E-W to WNW-ESE shortening as indicated by the maximum (blue bars) principal strain axes (Fig. 5). Moreover, within the lobe of contraction strain below the surface pop-up, the minimum principal strain axes (red bars) clearly show sub-vertical elongation in the cross section NS2 (Fig. 6e). We can also find that the contractional strain in this lobe increased downwards from 1×10^{-6} (6 km depth) to 1×10^{-5} (14 km depth) near the co-seismic fault plane.

On the other hand, we also observed a radial pattern of dilatational strain axes (Fig. 5a and 5b), which seemingly implies “radial deformation” characteristics of dilatation strain, around the surface coseismic pop-up area at the uppermost 0–2 km surface level.

Combining the “squeezing” contraction strain at the deeper part (5–14 km) below the surface coseismic pop-up, with the dilatation strain in the uppermost part (0–2 km), we argue that the fluid pore-pressure has high potential to be increased co-seismically in the bottom reservoir of the mud diapir MD-3, which is considered to lie at the depth of 5–6 km near the regional decollement. Although only the uppermost part of the contraction might influence the bottom of the MD-3, we interpret that the fluids were squeezed and raised upwards into the diapir through sub-vertical plumbing systems. This may allow fluid and gas pumping up within the MD-3 system, with effects propagating up to the surface pop-up.

5.3. Coulomb stress transfer on three major parallel mud diapirs

The results of our test for calculation of normal stress changes on three mud diapirs, which are technically treated as three vertical faults, were plotted in Fig. 8. In this figure, the negative normal stress changes (contraction, blue color) occur on the two western arrays of mud diapirs (in MD-1 and MD-2), suggesting clamping status for stress transfer on these two mud diapirs from top to bottom. On the other hand, on the easternmost mud diapir MD-3 around the co-seismic pop-up area, it shows compressive normal stress (blue color) in the deeper part (5–6 km) and the extension (red color) in the shallower part (0–3 km). This is consistent with the interpretation of the co-seismic uplift area that 1) the increased fluid pressure in the base or reservoir of the mud diapir/mud volcano (5–6 km depth) may promote its fluid/gas migration and 2) dilatation in the shallow part allowed the mud diapir to expand and migrate upward to near surface level.

Note that the maximum normal stress changes (clamping value $\Delta\sigma_n$ = -1 bar), acting on these structures, infer an increase of pore pressure for undrained condition Δp, which was estimated to be close to 1 bar, according to the formula $\Delta p = - B\Delta\sigma_n$ (Stein and Lisowski, 1983; Stein et al., 1992; King et al., 1994), where B is the Skempton coefficient (about 1 for mud).

6. Discussion

6.1. Cascade effects from coseismic strain change, mud diapiring to surface uplift

The mechanism(s) that cause the coseismic surface deformation of a 10 x15 km pop up by the Meinong earthquake have been under debate in the previous studies. One of the proposed mechanisms was the slip of ‘an unknown fault’ located a few kilometers above the main causative fault (Huang et al., 2016), likely near the depth of the regional fold-thrust decollement. However, there is no clear or solid geological constrain on this suspected blind fault, and the nature of such fault zone remains unknown. Second, Le Béon et al. (2017) proposed a shallowly west-dipping backthrust, located below the surface uplift, as the causative structure. Again, no direct evidence of the existence of this blind back-thrust can be provided as well. In this study, the location of the arrays of the mud volcanoes coincides with the area of co-seismic uplift, leading to the newly interpreted mechanism: mud diapiring.

The active, vigorous mud diapirism has been proposed to explain the rapid interseismic surface vertical motion in the fold-thrust belt of southwestern Taiwan (Ching et al., 2016; Tsukahara and Takada, 2018), which also caused various damages on surface human constructions around MDs/MVs areas (including MD-1, MD-2, MD-3 and MD-4) (Chen and Liu, 2000; Chen et al., 2014). Elsewhere in the world, MDs/MVs have also been recognized as a process that may be interplayed with seismic activity. For instance, Kadirov et al. (2005) and Bonini et al. (2016) used coseismic strain change to compare with the occurrence of mud volcanoes and proposed that volumetric contraction of deep fluid reservoirs promoted the response of mud volcanoes during the 2000 Baku earthquakes (Mw 6.8 and 6.5) in Azerbaijan.

Here we emphasize the role of MD/MV in co-seismic deformation. We argue that the 2016 Meinong co-seismic surface uplift was coupled with substantial mud diapiring in the mudstone area. As mentioned above, one of the mud volcanoes (Wushanting) above the MD-3 erupted coseismically, which provides additional supportive evidence for co-seismic triggered activity of MD-3. We interpret the aforementioned “squeezing” characteristics of the principal strain axes of the contraction

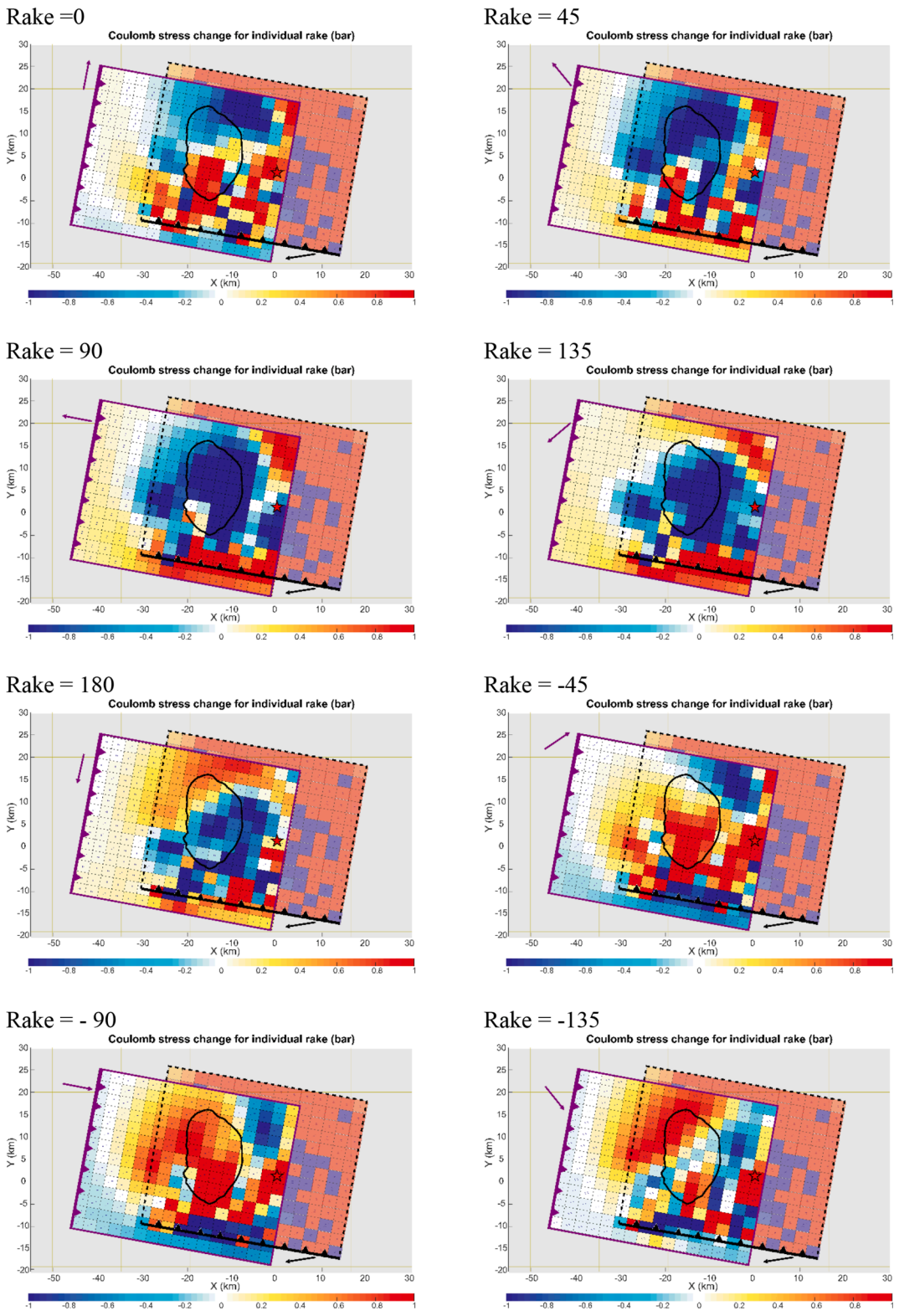

Fig. 9. Results of calculation of Coulomb stress changes on the regional fold-thrust decollement with different rakes of slip resolved from the source fault (lighted colors show the Coulomb stress changes on source fault). We can find that the Meinong earthquake significantly increased the Coulomb stress on the decollement at the depth of 5–7 km below the surface pop-up area (black contour), for the cases of normal faulting (rake = −90) or oblique right-lateral normal faulting (rake = −45). As a result, the Coulomb stress change does not favor triggered 'thrust' slip on the regional decollement under the surface pop-up. See main text for more explanations.

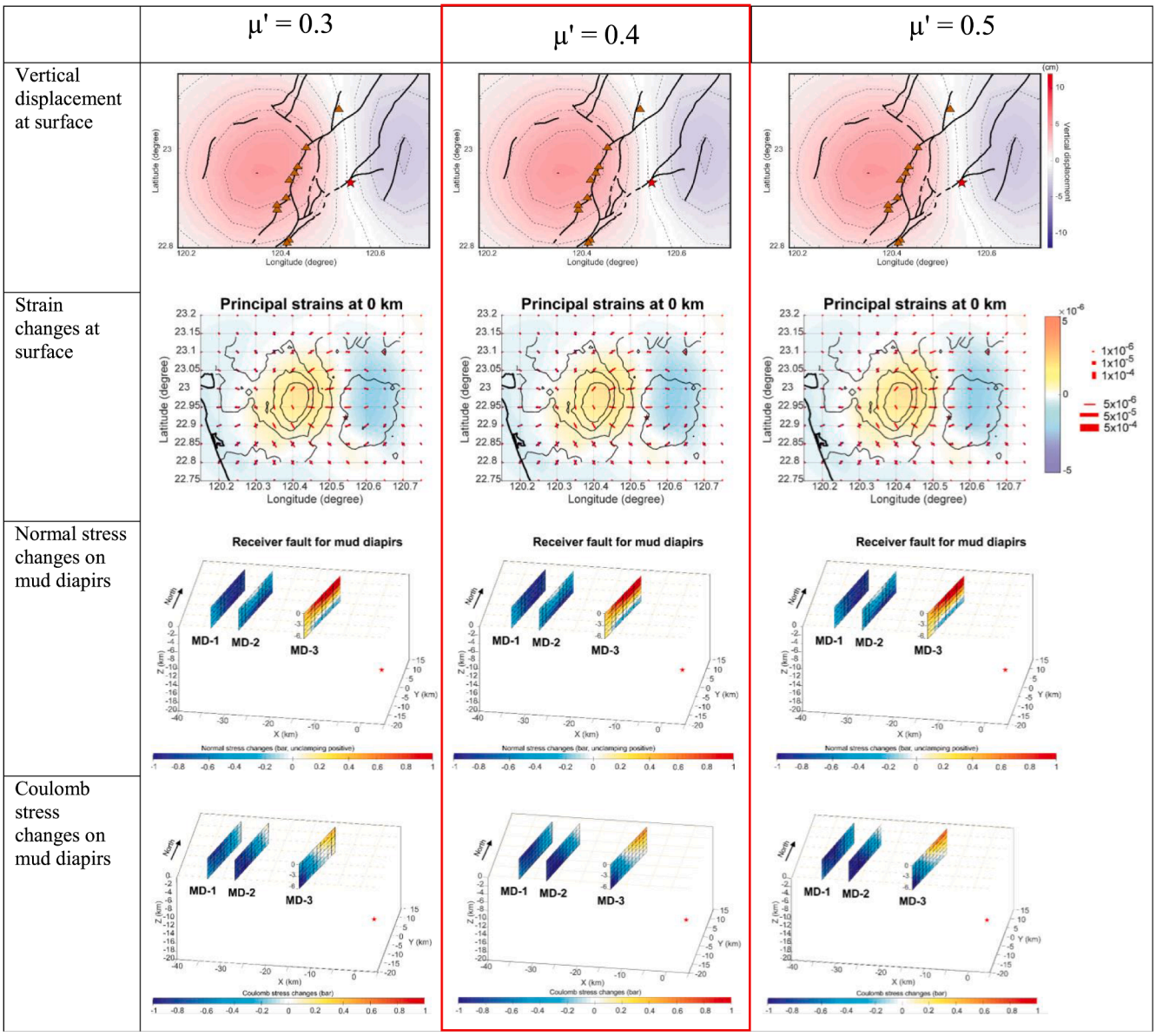

Fig. A1. Results of calculation of a) vertical displacement, b) volumetric strain changes at surface, c) normal stress changes and d) coulomb stress changes on three NNE-trending regional mud diapirs (MD-1, MD-2 and MD-3) with different values of coefficient of friction, μ' = 0.3, μ' =0.4 and μ' = 0.5. The results show different values of μ' did not play significant role on Coulomb stress change. Note that in this study, we adopt μ' =0.4.

lobe following the Meinong earthquake gives a favorable condition that generated the increase of fluid pore-pressure at the base of the MD-3. And then the fluid can be transmitted upwards along the network of mud/fluid/gas conduits of the MD-3 in the surface uplift area. Using the 2002–2010 GPS and leveling measurements, Ching et al. (2016) inferred that the activity of mud diapir is responsible of the high interseismic uplift rates up to 18 mm/yr in the mudstone area of southwestern Taiwan. Using 2007–2011 InSAR data in the same area, Tsukahara and Takada (2018) obtained even higher aseismic uplift rates (up to 37 mm/yr) and interpreted them to result mainly from mud diapiring. The InSAR data also indicated this interseismic uplift area was aligned in the N-S direction with a length of ~25 km, generally consistent with the main alignment of mud volcanoes in the region.

Earlier surveys of gravity and seismic reflection in the years of 1960 s and 1970 s indicated a series of subsurface en-echelon anticlines trending NNE-SSW in the Coastal Plain of southwestern Taiwan (Pan, 1968; Hsieh, 1972). In the cores of the anticlines, the lack of reflectors in the seismic reflection profiles (Hsieh, 1972) may indicate strong fluid networks that is a result of intrusion of mud/fluid/gas (i.e., mud diapiring) and/or conduits of mud volcanoes. The presence of an abnormally high fluid pressure zone in the mudstone of Southwest Taiwan is also supported by borehole observation and analysis (Yuan et al., 1987). At the Lungchuan and Tainan anticlines, gravity measurements and seismic Vp/Vs analysis indicates significant increase of mud density (Huang et al., 2004), which implies hardening of mudstone, probably a result of fluid draining/undraining processes. Moreover, the relatively large density contrast (~0.3–0.5 g cm^{-3}) was observed between the rocks in the anticline cores and those outside of anticlines (Hsieh, 1972), implying that the hardened mudstone into the anticlines is probably due to dehydration of clay minerals. Similar hardened rocks in anticline cores were also inferred recently form MVs and MDs, based on gravity data in the offshore area of Southwest Taiwan (Doo et al., 2015).

In this study, we find that the main shock of the Meinong earthquake is able to produce a major contraction strain in an area with a diameter of 6–8 km. The location of this contraction lobe was sitting above the causative fault plane, about 5–14 km below the surface uplift (an array

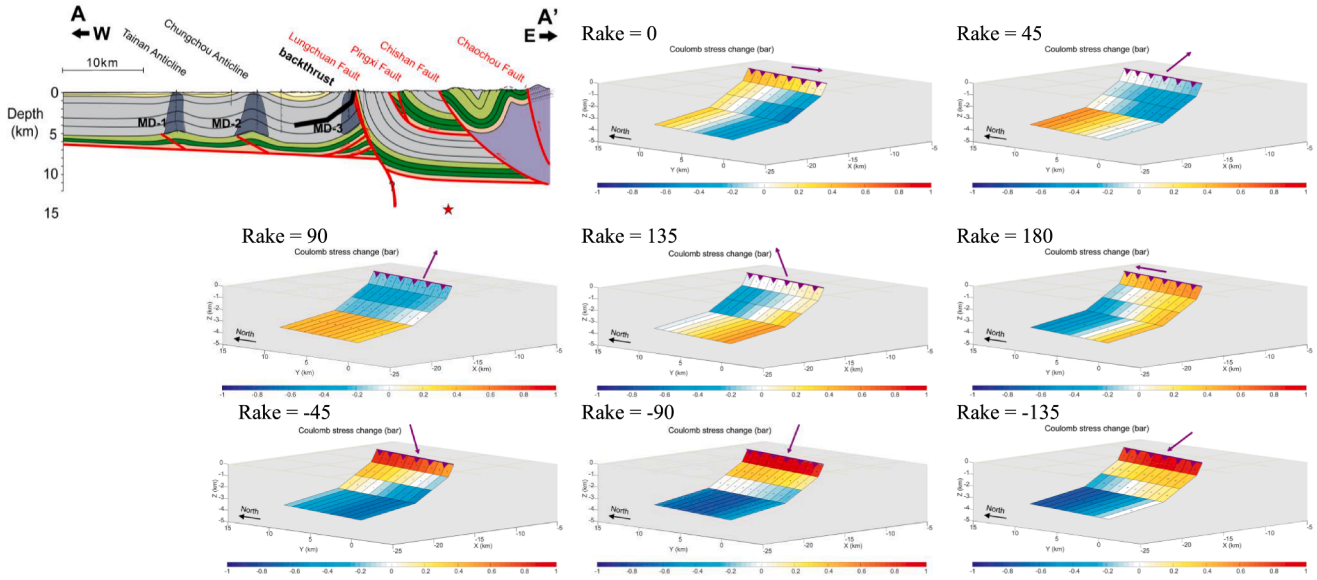

Fig. A2. Results of calculation of Coulomb stress changes on the Lungchuan backthrust with different rakes of slip. Heavy black line denote the backthrust in the geological profile. We can find that the Meinong earthquake significantly increased the Coulomb stress on the backthrust for the cases of normal faulting (rake = -90) or oblique strike-slip with normal faulting (rake = -45 and rake = -135). As a result, the Coulomb stress change does not favor triggered 'thrust' slip on the backthrust under the surface pop-up. See main text for more explanations.

of mud volcanoes) area. This contractional strain change may increase fluid pressure at the bottom of the MD-3 (at depth of 5–6 km), albeit in the uppermost contraction lobe. We thus propose that this stress/strain perturbation would enhance the activity of the network of mud/fluid/gas of MDs/MVs in the co-seismic pop-up area. The geochemistry signals of MVs surface fluids (with high Cl, B, Ba, and Li contents) extracted during the interseismic period also implied a high-pressure, fluid-rich source, coming from the depths of about 2–5 km (You et al., 2004; Chao et al., 2011; Chao et al., 2013). This is consistent with the relatively high Vp/Vs ratios (~2.0) around the contraction strain lobe (Huang et al., 2014). The coseismic uplift area is most likely associated with the fluid-rich pressurized region in the subsurface, which favors that stress perturbation plays an important role in the crust deformation in the region.

6.2. Coulomb stress transfer on the fold-thrust decollement or other faults?

We also tested whether triggering may potentially happen on the decollement of the fold-thrust belt in the study area, mainly because it is near the inferred base of the reservoir of the MDs/MVs in the study area. In terms of the distribution of the aftershocks of the Meinong earthquake, in addition to the three main clusters in three zones as we mentioned earlier, however, some aftershocks seem to occur around the decollement (Wen et al., 2017). Based on the regional geological information we set up the main orientation parameters of the decollement as following: strike = N10°E, dip = 5°E and depths = 5–9 km. We then calculated Coulomb stress changes on the decollement as a 'receiver' fault for the Meinong earthquake case considering different scenarios for slip direction (i.e., different rakes). The resulting pattern of stress change are shown in Fig. 9. The Meinong earthquake increased the Coulomb stress on the decollement for normal faulting (rake = -90) or oblique right-lateral normal faulting (rake = -45). This suggests that the ΔCFS due to the co-seismic slip Meinong earthquake unlikely triggered thrust slip on the regional decollement under the co-seismic uplift area.

We then tested possible triggered slip on the Lungchuan backthrust, which was interpreted to explain the coseismic pop-up deformation (Le Béon et al. (2017). The authors interpreted this structure in their profile with a dip of 35-40°W, a depth from near surface down to 4 km deep, a strike of N10° E and a length of 8–10 km (Fig. A2). We thus calculated Coulomb stress changes due to Meinong earthquake on this backthrust as a 'receiver' fault. With different scenarios for slip direction (i.e., different rakes) (Fig. A2). The Meinong earthquake would increase the Coulomb stress on the backthrust in case of normal faulting (rake = -90) or oblique strike-slip with normal faulting (rake = -45 and rake = -135). This suggests that the static stress transfer ΔCFS due to the co-seismic slip of the Meinong earthquake does not favor thrust slip in this suspected backthrust under the co-seismic uplift area.

Finally, we tested normal stress changes on the Lungchuan thrust fault, a major ramp emanated from the thrust décollement around the surface pop-up area (Fig. A3). We obtained a high positive value of normal stress changes at the uppermost 0–4 km on the Lungchuan fault, indicating the structure is favorably oriented for being dilated/reactivated by the co-seismic stress changes. We suspect this may favor the channelling of fluids upwards, such as the case of Mw 7.2 and Mw 7.4 earthquakes in 2004 near Kumano Basin, Japan (Bonini, 2019), presumably on the footwall side (mudstone area) of the fault. As a result, the unclamping normal stress at the shallow few kilometers on the Lungchun fault gives another favorable condition for the upraising of fluid/gas/mud in the mudstone area during the Meinong earthquake.

6.3. Comparisons between 2016 Meinong and 2010 Jiashian earthquakes

Prior to the 2016 Meinong earthquake, a moderate earthquake with a similar magnitude occurred in the nearby area, in 2010. In particular, the 2010 M_L 6.4 Jiashian earthquake, with a hypocentral depth of 23 km, occurred ~20 km east of the 2016 Meinong earthquake (Fig. A4), however, no observable co-seismic surface pop-up or subsidence occurred. In order to compare the coseismic stress/strain changes on the shallow crust between these two earthquakes, we calculated the 3D principal strains and volumetric coseismic strains due to the Coulomb stress change of the ML 6.4 Jiashian earthquake (Fig. A4). In this case, we adopted the coseismic slip model proposed by Lee et al. (2013). The magnitude of coseismic strain changes induced by the Jiashain earthquake were estimated to be around 10^{-6}–10^{-7} (Fig. A4c and A4d), which is approximately one order of magnitude smaller than the coseismic strain changes generated by the Meinong earthquake (10^{-5}–10^{-6}). Unlike the "squeezing" characteristics of the principal

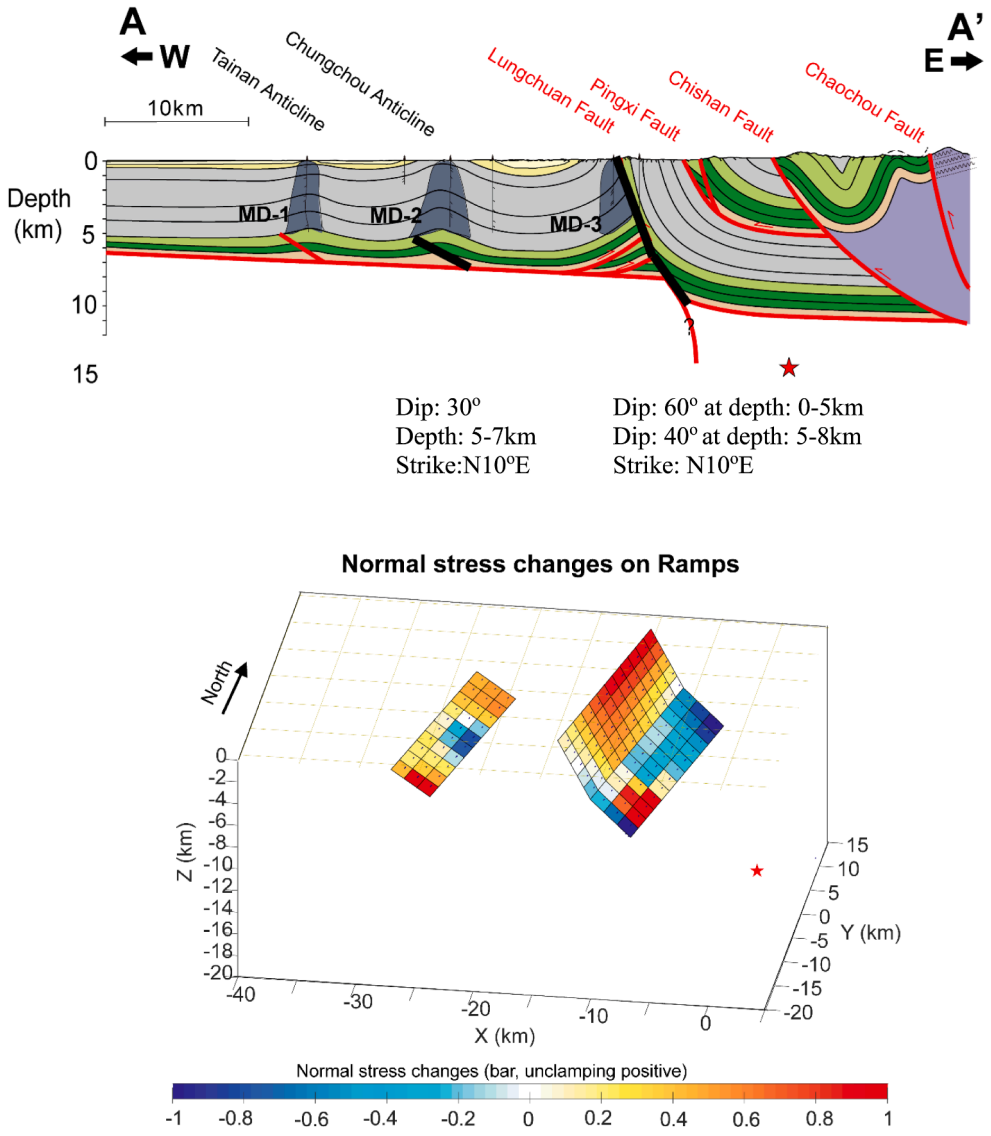

Fig. A3. Results of calculation of normal stress changes on the thrust ramps emanated from the thrust décollement around the surface pop-up area: the Lungchuan fault (with different scenarios for geometry). The results predict 1) unclamping normal stress changes on the upper 0–4 km of the Lungchuan fault and 2) clamping normal stress changes on the lower part (5–8 km deep) of the fault. See main text for more explanations.

strain axes and/or an upward intruding diapir induced by the Meinong earthquake, the Jiashian earthquake did not generate a similar pattern. No substantial surface vertical displacement happened during and after the Jiashian earthquake, suggesting that the activity of mud diapirs and mud volcanoes was not promoted. It thus appears that stress/strain increase was insufficient to influence fluid pressurization in the mudstone area.

7. Conclusions

By calculating the Coulomb stress change of the 2016 Mw 6.4 Meinong earthquake, we obtained 3D strain tensors, which represented volumetric coseismic strain changes in a 3D space with 5 × 5 × 2 km grids. We also tested the Coulomb stress transfer on several 'receiver fault' systems in the epicentral area: a) the three arrays of mud diapirs, b) the regional thrust decollement, c) a suspected backthrust, and d) one regional major thrust. In an attempt to interpret the surface co-seismic pop up above the mud diapir MD-3, we were able to draw the following conclusions.

(1) At the shallow part near the surface level at 0–3 km, there is a dominant dilatation strain with the radial pattern of the maximum lengthening principal strain axes in and around the surface coseismic uplift area (15 × 10 km), with a maximum coseismic uplift of 12 cm.
(2) We obtained substantial contractional strain (10^{-5}–10^{-6}) in a lobe, ~6 km in diameter, situated right below the coseismic surface uplift area at the depths of 5–14 km, which also revealed the "squeezing" characteristics of the principal strain.
(3) We adopted the array of a series of MDs/MVs in the uplift area as a 'receiver fault' to calculate the Coulomb stress transfer onto it. The results of the MD-3 showed that unclamping stress changes (up to 1 bar) occurred at shallow depth (0–4 km) while clamping stress changes (up to −1 bar) occurred in deeper depths (5–6 km).
(4) Our results showed that the Coulomb stress transfer caused by coseismic slip unlikely promoted triggered thrust slip on several local thrust faults, including the regional decollement of fold-thrust belt and the suspected backthrust. On the other hand, the unclamping stress of the Lungchuan fault at 3 km depth favors the channelling of the fluid/gas upward close to the pop-up area.

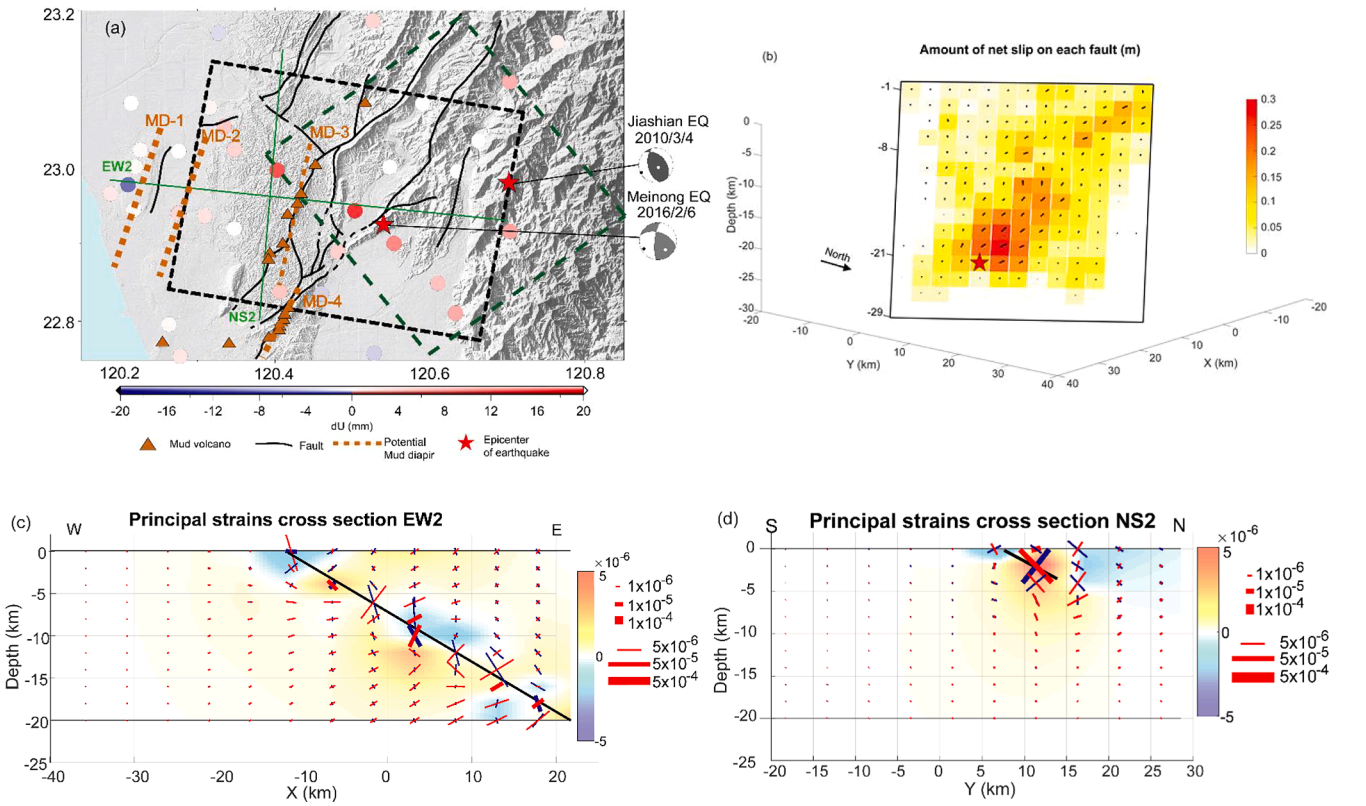

Fig. A4. Characteristics of the 2010 ML 6.4 Jiashian earthquake. (a) GPS coseismic vertical displacements (after Hsu et al., 2011). Note that the vertical motion was in the slim range of [-2, 2] cm. The dashed black and dashed green rectangles indicate the source fault models of Meinong and Jiashian earthquakes, respectively. Green lines are location of cross sections in Fig. A4c and A4d. (b) The model adopted for coseismic slip distribution of the Jiashian earthquake (after Lee et al., 2013). (c) and (d) Results of calculation of strain change due to 2010 Jiashian earthquake. Distribution of 3-D principal strain axes are projected on to the vertical planes. Red color: dilatation strain. Blue color: contraction strain. The causative fault is indicated as black heavy line. We can observe that the strain changes induced by the Jiashian earthquake were in the range of 10^{-6}–10^{-7}, which is tens time smaller than those from the Meinong earthquake.

(5) Considering the MDs/MVs arrays in the locally rich mudstone, we interpret that the 2016 Meinong earthquake coseismic surface uplift was triggered by the activity of MD/MV structures. The MDs/MVs were likely reactivated by an increase of contraction strain in the basal reservoir of the mud diapirs around 5–6 km depth. The mud/fluid/gas raised upward through the network of conduits of MD-3 to cause the pop-up deformation at the surface level.

CRediT authorship contribution statement

Hue Anh Mai: Conceptualization, Data curation, Formal analysis, Investigation, Visualization, Writing - original draft. **Jian-Cheng Lee:** Conceptualization, Formal analysis, Funding acquisition, Investigation, Project administration, Resources, Supervision, Validation, Writing - original draft, Writing - review & editing. **Kate Huihsuan Chen:** Conceptualization, Validation. **Kuo-Liang Wen:** Supervision.

Declaration of Competing Interest

The authors declare that they have no known competing financial interests or personal relationships that could have appeared to influence the work reported in this paper.

Acknowledgements

We are grateful for many constructive comments and suggestions from Chung-Han Chan and an anonymous reviewer, which substantially helped to improve the manuscript. This research was supported by the Ministry of Science and Technology (MOST) of Taiwan (grants MOST 107-2116-M-001 -026 -MY3). This is also part of the PhD dissertation of the first author. A part of the scholarship for the first author is under the Taiwan International Graduate Program (TIGP) — Earth System Science Program, between Academia Sinica, Taiwan and National Central University, Taiwan. This is a contribution of Institute of Earth Sciences, Academia Sinica, IESAS-2393.

Appendix A

See Figs. A1–A4.

Appendix B. Supplementary material

Supplementary data to this article can be found online at https://doi.org/10.1016/j.jseaes.2021.104847.

References

Albano, M., Barba, S., Solaro, G., Pepe, A., Bignami, C., Moro, M., Saroli, M., Stramondo, S., 2017. Aftershocks, groundwater changes and postseismic ground displacements related to pore pressure gradients: Insights from the 2012 Emilia-Romagna earthquake. J. Geophys. Res. Solid Earth 122, 5622–5638. https://doi.org/10.1002/2017JB014009.

Angelier, J., Chang, T.-Y., Hu, J.-C., Chang, C.-P., Siame, L., Lee, J.-C., Deffontaines, B., Chu, H.-T., Lu, C.-Y., 2009. Does extrusion occur at both tips of the Taiwan collision belt? Insights from active deformation studies in the Ilan Plain and Pingtung Plain regions. Tectonophysics 466, 356–376.

Babayev, G., Tibaldi, A., Bonali, F.L., Kadirov, F., 2014. Evaluation of earthquake-induced strain in promoting mud eruptions: the case of Shamakhi–Gobustan–Absheron areas, Azerbaijan. Nat. Hazards 72, 789–808.

Barber, A., Tjokrosapoetro, S., Charlton, T., 1986. Mud volcanoes, shale diapirs, wrench faults, and melanges in accretionary complexes, eastern Indonesia. AAPG Bull. 70, 1729–1741.
Bonini, M., 2019. Seismic loading of fault-controlled fluid seepage systems by great subduction earthquakes. Sci. Rep. 9, 11332.
Bonini, M., Rudolph, M.L., Manga, M., 2016. Long- and short-term triggering and modulation of mud volcano eruptions by earthquakes. Tectonophysics 672–673, 190–211.
Brown, K.M., 1990. The nature and hydrogeologic significance of mud diapirs and diatremes for accretionary systems. J. Geophys. Res. Solid Earth 95, 8969–8982.
Chang, S., Chi, W., 1983. Neogene nannoplankton biostratigraphy in Taiwan and the tectonic implications. Petrol. Geol. Taiwan 19, 93–147.
Chao, H.-C., You, C.-F., Liu, H.-C., Chung, C.-H., 2013. The origin and migration of mud volcano fluids in Taiwan: Evidence from hydrogen, oxygen, and strontium isotopic compositions. Geochimica et Cosmochimica Acta 114, 29–51.
Chao, H.-C., You, C.-F., Wang, B.-S., Chung, C.-H., Huang, K.-F., 2011. Boron isotopic composition of mud volcano fluids: Implications for fluid migration in shallow subduction zones. Earth Planet. Sci. Lett. 305, 32–44.
Chen, S.-C., Hsu, S.-K., Wang, Y., Chung, S.-H., Chen, P.-C., Tsai, C.-H., Liu, C.-S., Lin, H.-S., Lee, Y.-W., 2014. Distribution and characters of the mud diapirs and mud volcanoes off southwest Taiwan. J. Asian Earth Sci. 92, 201–214.
Chen, Y.-G., Liu, T.-K., 2000. Holocene uplift and subsidence along an active tectonic margin southwestern Taiwan. Quat. Sci. Rev. 19, 923–930.
Chinese Petroleum Corporation (CPC), 1989. The Geological Map of Tainan (scale 1: 100,000). Taiwan Petroleum Exploration Division Publication, Chinese Petroleum Corporation, Taiwan, ROC.
Ching, K.-E., Gourley, J.R., Lee, Y.-H., Hsu, S.-C., Chen, K.-H., Chen, C.-L., 2016. Rapid deformation rates due to development of diapiric anticline in southwestern Taiwan from geodetic observations. Tectonophysics 692, 241–251.
Ching, K.-E., Johnson, K.M., Rau, R.-J., Chuang, R.Y., Kuo, L.-C., Leu, P.-L., 2011. Inferred fault geometry and slip distribution of the 2010 Jiashian, Taiwan, earthquake is consistent with a thick-skinned deformation model. Earth Planet. Sci. Lett. 301, 78–86.
Chiu, J.-K., Tseng, W.-H., Liu, C.-S., 2006. Distribution of gassy sediments and mud volcanoes offshore southwestern Taiwan. TAO. Terrestrial, Atmospheric and Oceanic Sciences 17, 703.
CWB, 2016. Meinong earthquake. Taiwan Central Weather Bureau. www.cwb.gov.tw.
Dadson, S.J., Hovius, N., Chen, H., Dade, W.B., Hsieh, M.-L., Willett, S.D., Hu, J.-C., Horng, M.-J., Chen, M.-C., Stark, C.P., Lague, D., Lin, J.-C., 2003. Links between erosion, runoff variability and seismicity in the Taiwan orogen. Nature 426, 648–651.
Deville, E., Battani, A., Griboulard, R., Guerlais, S., Herbin, J.P., Houzay, J.P., Muller, C., Prinzhofer, A., 2003. The origin and processes of mud volcanism: new insights from Trinidad. Geol. Soc., London, Special Publications 216, 475–490.
Doo, W.-B., Hsu, S.-K., Lo, C.-L., Chen, S.-C., Tsai, C.-H., Lin, J.-Y., Huang, Y.-P., Huang, Y.-S., Chiu, S.-D., Ma, Y.-F., 2015. Gravity anomalies of the active mud diapirs off southwest Taiwan. Geophys. Supp. Monthly Not. Roy. Astron. Soc. 203, 2089–2098.
Grecksch, G., Roth, F., Kümpel, H.J., 1999. Coseismic well-level changes due to the 1992 Roermond earthquake compared to static deformation of half-space solutions. Geophys. J. Int. 138, 470–478.
Ho, C.-S., 1982. Tectonic evolution of Taiwan: explanatory text of the tectonic map of Taiwan. Ministry of Economic Affairs, Republic of China.
Hsieh, S., 1972. Subsurface geology and gravity anomalies of the Tainan and Chungchou structures of the coastal plain of southwestern Taiwan. Petrol. Geol. Taiwan 10, 323–338.
Hsu, Y.-J., Yu, S.-B., Kuo, L.-C., Tsai, Y.-C., Chen, H.-Y., 2011. Coseismic deformation of the 2010 Jiashian, Taiwan earthquake and implications for fault activities in southwestern Taiwan. Tectonophysics 502, 328–335.
Huang, H.-H., Wu, Y.-M., Song, X., Chang, C.-H., Lee, S.-J., Chang, T.-M., Hsieh, H.-H., 2014. Joint Vp and Vs tomography of Taiwan: Implications for subduction-collision orogeny. Earth Planet. Sci. Lett. 392, 177–191.
Huang, M.-H., Tung, H., Fielding, E.J., Huang, H.-H., Liang, C., Huang, C., Hu, J.-C., 2016. Multiple fault slip triggered above the 2016 Mw 6.4 MeiNong earthquake in Taiwan. Geophys. Res. Lett. 43, 7459–7467.
Huang, S.-T., Yang, K.-M., Hung, J.-H., Wu, J.-C., Ting, H.-H., Mei, W.-W., Hsu, S.-H., Lee, M., 2004. Deformation front development at the northeast margin of the Tainan basin, Tainan-Kaohsiung area. Taiwan. Marine Geophysical Researches 25, 139–156.
Hui, G., Li, S., Wang, P., Zhu, J., Guo, L., Wang, Q., Somerville, I.D., 2018. Neotectonic implications and regional stress field constraints on mud volcanoes in offshore southwestern Taiwan. Mar. Geol. 403, 109–122.
Johnston, M.J.S., Borcherdt, R.D., Linde, A.T., Gladwin, M.T., 2006. Continuous Borehole Strain and Pore Pressure in the Near Field of the 28 September 2004 M 6.0 Parkfield, California, Earthquake: Implications for Nucleation, Fault Response, Earthquake Prediction, and Tremor. Bull. Seismol. Soc. Am. 96, S56–S72.
Jónsson, S., Zebker, H., Segall, P., Amelung, F., 2002. Fault Slip Distribution of the 1999 Mw 7.1 Hector Mine, California, Earthquake, Estimated from Satellite Radar and GPS Measurements. Bulletin of the Seismological Society of America 92, 1377–1389.
Kadirov, F.A., Lerche, I., Guliyev, I.S., Kadyrov, A.G., Feyzullayev, A.A., Mukhtarov, A.S., 2005. Deep Structure Model and Dynamics of Mud Volcanoes, Southwest Absheron Peninsula (Azerbaijan). Energy Explor. Exploit. 23, 307–332.
King, G.C.P., Stein, R.S., Lin, J., 1994. Static stress changes and the triggering of earthquakes. Bull. Seismol. Soc. Am. 84, 935–953.
Kopf, A.J., 2002. Significance of mud volcanism. Rev. Geophys. 40, 2-1-2-52.
Kroll, K.A., Cochran, E.S., Murray, K.E., 2017. Poroelastic properties of the Arbuckle Group in Oklahoma derived from well fluid level response to the 3 September 2016 M w 5.8 Pawnee and 7 November 2016 M w 5.0 Cushing earthquakes. Seismol. Res. Lett. 88, 963–970.
Ku, C.-Y., Hsu, S.-K., 2009. Crustal structure and deformation at the northern Manila Trench between Taiwan and Luzon islands. Tectonophysics 466, 229–240.
Kuo-Chen, H., Wu, F.T., Roecker, S.W., 2012. Three-dimensional P velocity structures of the lithosphere beneath Taiwan from the analysis of TAIGER and related seismic data sets. J. Geophys. Res.: Solid Earth 117, B06306. https://doi.org/10.1029/2011JB009108.
Le Béon, M., Huang, M.-H., Suppe, J., Huang, S.-T., Pathier, E., Huang, W.-J., Chen, C.-L., Fruneau, B., Baize, S., Ching, K.-E., 2017. Shallow geological structures triggered during the Mw 6.4 Meinong earthquake, southwestern Taiwan. Terr Atmos Ocean Sci 28, 663–681.
Lee, S.-J., Mozziconacci, L., Liang, W.-T., Hsu, Y.-J., Huang, W.-J., Huang, B.-S., 2013. Source complexity of the 4 March 2010 Jiashian, Taiwan, Earthquake determined by joint inversion of teleseismic and near field data. J. Asian Earth Sci. 64, 14–26.
Lee, S.J., Yeh, T.Y., Lin, Y.Y., 2016. Anomalously Large Ground Motion in the 2016 ML 6.6 Meinong, Taiwan, Earthquake: A Synergy Effect of Source Rupture and Site Amplification. Seismol. Res. Lett. 87, 1319–1326.
Li, Y.-H., 1976. Denudation of Taiwan Island since the Pliocene Epoch. Geology 4, 105–107.
Lin, J., Stein, R.S., 2004. Stress triggering in thrust and subduction earthquakes and stress interaction between the southern San Andreas and nearby thrust and strike-slip faults. J. Geophys. Res.: Solid Earth 109, B02303. https://doi.org/10.1029/2003JB002607.
Liu, C.-C., Yu, S.-B., 1990. Vertical crustal movements in eastern Taiwan and their tectonic implications. Tectonophysics 183, 111–119.
Liu, C.-S., Huang, I.L., Teng, L.S., 1997. Structural features off southwestern Taiwan. Mar. Geol. 137, 305–319.
Liu, C.-S., Schnurle, P., Wang, Y., San-Hsiung, C., Song-Chuen, C., Hsiuan, T.-H., 2006. Distribution and characters of gas hydrate offshore of southwestern Taiwan. Terrestrial, Atmospheric and Oceanic Sciences 17 (4), 615–644.
Lu, C.-Y., Malavieille, J., 1994. Oblique convergence, indentation and rotation tectonics in the Taiwan Mountain Belt: Insights from experimental modelling. Earth Planet. Sci. Lett. 121, 477–494.
Manga, M., Bonini, M., 2012. Large historical eruptions at subaerial mud volcanoes. Italy. Nat. Hazards Earth Syst. Sci. 12, 3377–3386.
Manga, M., Brumm, M., Rudolph, M.L., 2009. Earthquake triggering of mud volcanoes. Mar. Pet. Geol. 26, 1785–1798.
McIntosh, K., Nakamura, Y., Wang, T.K., Shih, R.C., Chen, A., Liu, C.S., 2005. Crustal-scale seismic profiles across Taiwan and the western Philippine Sea. Tectonophysics 401, 23–54.
Mouthereau, F., Lacombe, O., Deffontaines, B., Angelier, J., Brusset, S., 2001. Deformation history of the southwestern Taiwan foreland thrust belt: insights from tectono-sedimentary analyses and balanced cross-sections. Tectonophysics 333 (1-2), 293–322. https://doi.org/10.1016/S0040-1951(00)00280-8.
Okada, Y., 1985. Surface deformation due to shear and tensile faults in a half-space. Bull. Seismol. Soc. Am. 75, 1135–1154.
Okada, Y., 1992. Internal deformation due to shear and tensile faults in a half-space. Bull. Seismol. Soc. Am. 82, 1018–1040.
Pan, Y., 1968. Interpretation and seismic coordination of the Bouguer gravity anomalies obtained in southwestern Taiwan. Petrol. Geol. Taiwan 6, 197–208.
Peng, K.-Y., Lee, J.-C., Liu, C.-S., 2020. Structural Characteristics of Mud Diapir/Mud Volcano in an Accretionary Wedge Under Mountain Building: Connection Between Offshore and Onshore in Southwestern Taiwan. In: Annual meeting of Geophysical Society of Taiwan and Geological Society at Taipei, Taipei.
Qiu, Z., Shi, Y., 2003. Observations of remote coseismic stress step-changes. Sci. China, Ser. D Earth Sci. 46, 75–81.
Quilty, E.G., Roeloffs, E.A., 1997. Water-level changes in response to the 20 December 1994 earthquake near Parkfield, California. Bull. Seismol. Soc. Am. 87, 310–317.
Reilinger, R.E., Ergintav, S., Bürgmann, R., McClusky, S., Lenk, O., Barka, A., Gurkan, O., Hearn, L., Feigl, K.L., Cakmak, R., Aktug, B., Ozener, H., Töksoz, M.N., 2000. Coseismic and Postseismic Fault Slip for the 17 August 1999, M = 7.5, Izmit, Turkey Earthquake. Science 289, 1519–1524.
Savage, J.C., Prescott, W.H., 1978. Asthenosphere readjustment and the earthquake cycle. J. Geophys. Res. Solid Earth 83, 3369–3376.
Serpelloni, E., Anderlini, L., Belardinelli, M.E., 2012. Fault geometry, coseismic-slip distribution and Coulomb stress change associated with the 2009 April 6, Mw 6.3, L′Aquila earthquake from inversion of GPS displacements. Geophys. J. Int. 188, 473–489.
Shi, Z., Wang, G., Liu, C., 2013. Co-seismic groundwater level changes induced by the May 12, 2008 Wenchuan earthquake in the near field. Pure Appl. Geophys. 170, 1773–1783.
Stein, R., Lisowski, M., 1983. The 1979 Homestead Valley Earthquake Sequence, California: Control of Aftershocks and Postseismic Deformation. J. Geophys. Res. 88, 6477–6490.
Stein, R.S., King, G.C.P., Lin, J., 1992. Change in Failure Stress on the Southern San Andreas Fault System Caused by the 1992 Magnitude = 7.4 Landers Earthquake. Science 258, 1328–1332.
Suppe, J., 1981. Mechanics of mountain building and metamorphism in Taiwan. Mem. Geol. Soc. China 4, 67–89.
Teng, L.S., 1990. Geotectonic evolution of late Cenozoic arc-continent collision in Taiwan. Tectonophysics 183, 57–76.
Toda, S., Stein, R.S., Richards-Dinger, K., Bozkurt, S.B., 2005. Forecasting the evolution of seismicity in southern California: Animations built on earthquake stress transfer. J. Geophys. Res.: Solid Earth 110, B05S16. https://doi.org/10.1029/2004JB003415.

Toda, S., Stein, R.S., Sevilgen, V., Lin, J., 2011. Coulomb 3.3 Graphic-rich deformation and stress-change software for earthquake, tectonic, and volcano research and teaching—user guide. US Geol. Surv. open-file report 1060, 63.

Tsukahara, K., Takada, Y., 2018. Aseismic fold growth in southwestern Taiwan detected by InSAR and GNSS. Earth Planets Space 70 (52). https://doi.org/10.1186/s40623-018-0816-6.

Weaver, K.C., Cox, S.C., Townend, J., Rutter, H., Hamling, I.J., Holden, C., 2019. Seismological and Hydrogeological Controls on New Zealand-Wide Groundwater Level Changes Induced by the 2016 Mw 7.8 Kaikōura Earthquake. Geofluids 2019, ID9809458, https://doi.org/10.1155/2019/9809458.

Wen, S., Yeh, Y.L., Chang, Y.-Z., Chen, C.H., 2017. The seismogenic process of the 2016 Meinong earthquake, Southwest Taiwan. Terrest. Atmosph. Oceanic Sci. 28 (5), 651–662.

Westbrook, G., Smith, M., 1983. Long decollements and mud volcanoes: Evidence from the Barbados Ridge Complex for the role of high pore-fluid pressure in the development of an accretionary complex. Geology 11, 279–283.

Yassir, N.A., 1989. Mud volcanoes and the behaviour of overpressured clays and silts. PhD. thesis. University of London.

Yuan, J., Huang, S.-T., Chou, T.-F., Wu, J.-C., Lu, D.-L., 1987. The origin of the abnormal pressure zones in Southwestern Taiwan [in Chinese with English abstract]. Ann. Explor. Prod. (CPC) 10, 1–27.

You, C.-F., Gieskes, J.M., Lee, T., Yui, T.-F., Chen, H.-W., 2004. Geochemistry of mud volcano fluids in the Taiwan accretionary prism. Appl. Geochem. 19, 695–707.